An Acad Bras Cienc (2024) 96(Suppl. 2): e20240362 DOI 10.1590/0001-3765202420240362
Anais da Academia Brasileira de Ciências | *Annals of the Brazilian Academy of Sciences*
Printed ISSN 0001-3765 I Online ISSN 1678-2690
www.scielo.br/aabc | www.fb.com/aabcjournal

GEOSCIENCES

TerraSAR-X SAR data for classification of ice-free areas and glacier facies on Fildes Peninsula, King George Island, Antarctica

ANDRÉ M. DE ANDRADE, ROBERTO F.M. MICHEL, KÁTIA K. DA ROSA, ULISSES F. BREMER, CARLOS ERNESTO G.R. SCHAEFER & JEFFERSON C. SIMÕES

Abstract: The region of the Maritime Antarctic suffers significantly from climate change, resulting in regional warming and consequently affecting coverage. This study characterized three surface zones of Collins Glacier and three other zones in ice-free areas on the Fildes Peninsula, which has an area of 29.6 km². We used TerraSAR-X satellite images from 2014 to 2016 and analyzed the influence of meteorological and environmental conditions on these surface zones. We used five images from the TerraSAR-X satellite, three of these data were obtained during the same period of fieldwork. The classification considered three classes on the glacier (higher moisture, transition in moisture, and lower moisture) and three on the ice-free areas (wet snow, transition wet snow-bare ice, and bare ice), using Maximum Likelihood and ISODATA methods. In low-altitude glaciers with maritime influence, such as Collins, monitoring variations in surface zones is essential because the continuous increase in exposed ice may indicate potential retreat. The TerraSAR-X images enabled the classification of land features, highlighting the potential for continuous monitoring in the Maritime Antarctic, regardless of weather conditions and solar illumination.

Key words: Maritime Antarctic, classification, backscatter monitoring, Antarctic landscape.

INTRODUCTION

Since 1950, one of the highest rates of warming on the planet has been recorded in the Antarctic Peninsula, with an increase of approximately 0.5ºC per decade (Turner et al. 2013), highlighting that the warming of the Antarctic Peninsula during this period was more significant than in the entire Southern Hemisphere (Siegert et al. 2019). In the Antarctic ecosystem, regions located at lower latitudes, such as the South Shetland Islands, are among the most affected by the increase in surface air temperature (Skvarca & De Angelis 2003), disrupting the balance of this fragile ecosystem.

Climate change and meteorological variations affect the surface coverage of environments in the Maritime Antarctic (Andrade et al. 2015). However, the region presents logistical complexities for fieldwork, and the prevalence of cloudy conditions hinders monitoring by optical remote sensing. Due to these conditions, Synthetic Aperture Radar (SAR) data is an essential alternative for monitoring regions with such conditions (Andrade et al. 2015, Falk et al. 2016, Rosa et al. 2020, Simões et al. 2020).

Since 2000, several studies have been conducted in Antarctica using SAR radar data. On King George Island, Braun et al. (2000) used ERS-2 SAR data to delineate glacier zones, contributing to understanding how different radar zones interact with local environmental

conditions. Also, on King George Island, Andrade et al. (2015) used COSMO-SkyMed data for the classification and monitoring of periglacial environments and glaciers, while Falk et al. (2016) applied TerraSAR-X data to generate glaciological and hydrological parameters. Rosa et al. (2020) used Sentinel-1 data in conjunction with other orbital data to study the dynamics of land-terminating glaciers over 62 years, showing how geomorphological formations influence variations in the glaciers of this region.

Arigony-Neto et al. (2009) used ERS-1/2 and ASAR data to analyze the spatial and temporal variations in the Antarctic Peninsula region in the dry-snow line altitude. In the same area, Simões et al. (2020) used Sentinel-1 data to quantify changes in two glaciers, finding a strong correlation between the SAR data and atmospheric and oceanic warming trends in the area. As a consequence of climate change in the region, Mendes Jr et al. (2022) used Envisat ASAR data to detect glacier facies with greater accuracy, proposing a method that combined the Wet Snow Radar Zone classification proposed by Arigony-Neto et al. (2009) and the snowmelt retrieval algorithm, resulting in a classification with improved precision.

The aim of this study was to characterize surface zones on the Collins Glacier and ice-free areas of the Fildes Peninsula using multi-temporal data from the TerraSAR-X satellite between 2014 and 2016 and to assess the influence of meteorological and environmental conditions on these surface zones.

MATERIALS AND METHODS

Study Site

Fildes Peninsula is located in the southwestern part of King George Island in the Maritime Antarctica region (Figure 1). The peninsula covers 29.8 km^2 of ice-free area and has the largest ice-free surface on King George Island (Michel et al. 2014). In the Maritime Antarctic region, the Fildes Peninsula was among the first to exhibit ice-free areas after the last glacial maximum (Curl 1980).

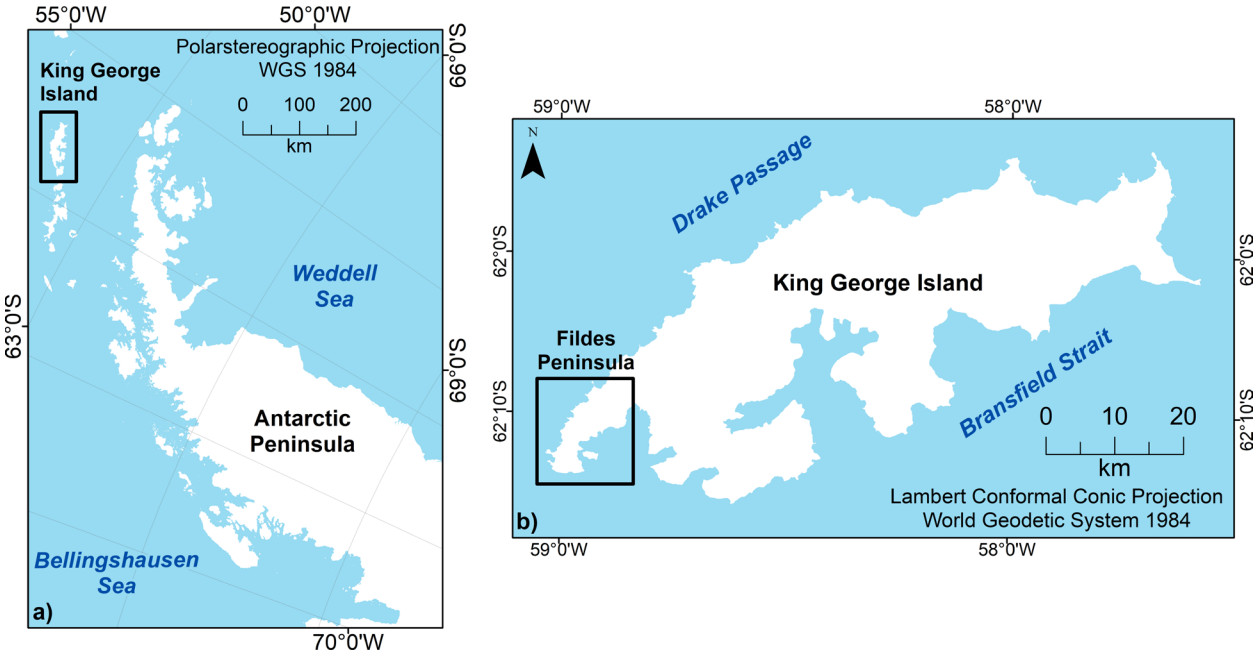

Figure 1. a) Location of the Antarctic Peninsula, and b) location of King George Island and highlight in Fildes Peninsula.

The landscape of the Fildes Peninsula has different environmental characteristics and is predominantly composed of eroded surfaces, flat surfaces on marine terraces, and higher surfaces inland (Curl 1980), forming a set of platforms with smooth and undulating relief. The retreat of the Collins Glacier has generated ice-free areas, with the transition from older regions at the beginning of the glacier retreat to the proglacial environment at the current edge of the Collins Glacier result. According to Michel et al. (2014), periglacial geomorphological processes such as solifluction, cryoturbation, and nivation are predominant in older areas. The predominant soil types in the study area are Cryosols, often cryoturbated, and to a lesser extent, Gleysols with gleyic characteristics (Michel et al. 2014). In this environment, pedogenetic processes are strongly influenced by the presence of fauna, which is an essential factor for the colonization and development of vegetation (Michel et al. 2006), in addition to the terrain configuration and soil moisture content (Peter et al. 2008).

The climate on Fildes Peninsula is maritime polar, characterized by solid winds predominantly from the north, northwest, and west directions (Vieira et al. 2014), along with frequent meteorological variations and milder temperatures. The climate is cold and humid, with an average annual air temperature of -2°C. The average air temperature can be slightly above 0°C during the summer and rarely drops below -12°C in winter (Wen et al. 1994). The rainfall varies between 350 and 500 mm throughout the year, predominantly during summer (Øvstedal & Smith 2001).

Characterization of surface zones

We conducted three fieldwork campaigns in February and March 2014, 2015, and 2016 to collect data for the research carried out in the study area. These studies aimed at monitoring the active layer of permafrost (Andrade et al. 2023) and vegetation cover (Andrade et al. 2018). In 2016, we acquired three scenes from the TerraSAR-X (TSX) satellite, coinciding with the fieldwork period. We obtained different types of data, including descriptions of surface snow, areas with higher moisture and temporary hydromorphism, and the geoenvironmental landforms of the study areas. These data were used to characterize the surface zones through TSX images.

This study used five scenes from the TSX satellite obtained at the Multi Look Ground Range Detected (MGD) processing level (Table I). The MGD data are provided with reduced speckle and higher accuracy in pixel resolution, resulting in equidistant pixels in azimuth and range resolution (DLR 2010). Because MGD products are raw data without any interpolation, it is possible to use specific parameters that

Table I. Technical information of the TerraSAR-X scenes used in this study.

Date	Time (UTC)	Orbit	Pass direction	Incidence Angle Range (°)	Polarization
10/03/2014	23:07:35	224	Ascending	20.630	HH
09/03/2015	08:23:00	257	Descending	42.877	HH
13/02/2016	08:23:07	288	Descending	31.342	HH
24/02/2016	08:23:07	289	Descending	48.221	HH
06/03/2016	08:23:08	290	Descending	48.388	HH

consider the peculiarities of the location, resulting in greater accuracy and precision in the extraction of physical data (DLR 2010).

The SAR data in its raw state has intrinsic errors due to the acquisition process by the orbital sensor. It is necessary to correct these errors to extract quantitative data, such as geophysical information from backscattering values, perform multi-temporal analysis, and compare SAR data acquired by different sensors. For the scenes to be suitable for extracting surface data, we performed three processing steps: radiometric calibration, speckle filtering (Yuan et al. 2018), and geometric correction.

We generated the DEM and then proceeded with the subsequent steps of characterizing the variation in snowmelt. The analysis of the spatial and temporal variation of the snow cover was performed using data extracted from the TSX images and validated through field-collected data, aided by a QuickBird image from 2008 and the landforms extracted from the DEM generated using a topographic map (IGM & INACH 1996).

The DEM was necessary for performing geometric and radiometric correction of SAR images and providing essential data for analyzing surface dynamics. The DEM of Fildes Peninsula was generated from contour lines with a 5 m equidistance from the topographic map of Fildes Peninsula (IGM & INACH 1996). The altimetric data from the contour lines were automatically digitized on a 32-inch screen, allowing a high level of zoom to evaluate the results, a method used to convert analog data into digital format.

We used the Topo to Raster interpolator with the Locally Adaptive Gridding method proposed by Hutchinson (1989). This interpolator was created to perform interpolations that utilize drainage characteristics, flow lines, elevation point grids, and other spatial data with irregular distribution in its model. We used the drainage network data of the Fildes Peninsula as a weighting factor in the interpolation process, resulting in a modeled surface based on elevation and the drainage network. The interpolation of the altimetric data was conducted in two steps: first, the algorithm generated the generalized morphology of the surface based on the values of the contour lines, and subsequently, the algorithm utilized the altimetric information from the contour lines to create the three-dimensional terrain forms. The DEM generated from the contour lines has a spatial resolution of 1 meter.

The SAR data have radiometric errors due to fluctuations in transmitted signal power, receiver gains, noise, and antenna illumination pattern (Freeman 1992). Radiometric normalization was performed for each pixel based on the antenna pattern, and surface information from reference points of the DEM was used (DLR 2010). The surface of the SAR scene was simulated based on topographic parameters extracted from the DEM and supplemented with attributes from the satellite flight path and illumination geometry (Freeman 1992).

The pixel values of the TSX raw data were related to terrain backscatter. These values were converted to radar backscatter (σ°) using the values of a surface projected onto the slant range as a reference and transforming the pixel values to decibel (dB) units.

We used the DEM for radiometric calibration and geometric correction of the TSX data, both with 1 m spatial resolution, and the interpolation applied to the pixels and the DEM used the nearest neighbor method. The data generated from geometric correction have higher precision in the pixel position, minimizing the effects of recurrent relief distortions.

Speckle is the random noise that generates the pattern of light and dark grey values in SAR data. This noise reduces the image quality and hinders the surface interpretation of targets.

Although it is not possible to completely remove speckle, we used a median convolution filter to reduce its effects in all TSX scenes. This filter was chosen because it produces minimal modification to the edges of the targets (Richards & Jia 2006). The filter was applied with 3x3 and 5x5 windows, and based on the statistical variability and variance rates of the data, the best results were obtained with the 5x5 window (Arigony-Neto et al. 2009, Andrade et al. 2015). The digital processing steps of the TSX images were performed using the Next ESA SAR Toolbox (NEST) software. Figure 2 displays the five TSX scenes already subjected to the processing steps.

To generate the terrain shape, we utilized the method proposed by Moore et al. (1991) and the Matrix Calculator tool, where we intersected the features of vertical and horizontal curvature, resulting in common areas for each curvature combination. Afterward, the terrain shape was segmented based on the orientation of the slopes, using azimuth values and the degree of slope for this procedure.

To assess snow melt during the ablation period on Collins Glacier and in the ice-free areas of Fildes Peninsula, we used the five TSX images, surface snow cover data, and the DEM. The albedo data recorded in the field using the CNR4 radiometer was applied to identify periods of surface snow cover and characterize the physical states of the snow according to albedo values. Albedo variations were also used to try to estimate the moisture content and physical state conditions of the snow.

The main surface classes that compose the Fildes Peninsula are exposed soil, rocks, snow, ice, vegetation cover, and water bodies. Some targets have characteristics that make their backscattering similar, and under these conditions, the water content in each target will be essential to differentiate the backscatter from the targets. This pattern results in classes that are not very heterogeneous, making the classification of TSX data difficult. Among these targets, snow and ice exhibit high temporal and spatial variability, mainly due to fluctuations resulting from changes in the physical state of water. The other targets, especially vegetation and permanent lakes, do not show significant variations in their configurations over short intervals (Andrade et al. 2015).

To enhance the ability to differentiate surface targets, we chose to segment the image into two portions, one encompassing the glacier area and the other the ice-free area. Although the two portions are distinct, both have targets with similar physical characteristics due to the presence of snow and ice, which result in the overlap of some backscattering ranges, thus reducing the accuracy of the classification.

The classification considered three classes on the glacier (wet snow, transition wet snow to bare ice, and bare ice) and three classes in ice-free areas (surface with higher moisture content, transition surface in moisture content, and surface with lower moisture content). Backscatter thresholds for classifying surface zones were proposed by Andrade et al. (2015). We included transition classes both on the glacier and in ice-free areas due to the 1 m spatial resolution of the TSX images and because we had a set of five images obtained on different dates. The transition classes, both on the glacier and in the ice-free areas, enable the differentiation of surfaces covered by snow and ice with greater melting potential and also detect surfaces with liquid water transitioning to a freezing condition.

The supervised classification was performed using the Maximum Likelihood method, and based on the backscatter of the selected samples, the algorithm recognized the backscatter patterns of the surface targets. Based on the backscatter

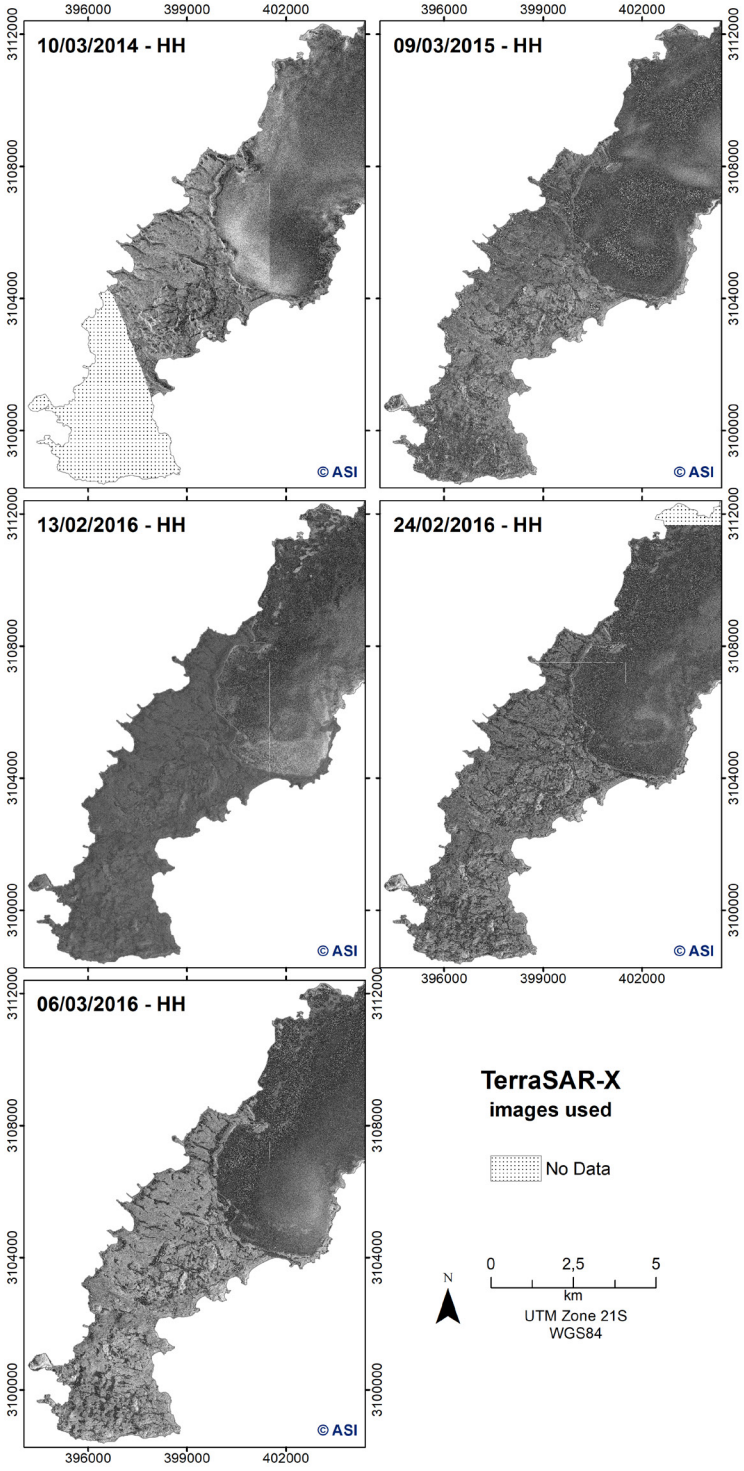

Figure 2. Images from the TerraSAR-X satellite of the Fildes Peninsula used in this study.

pattern of the samples, the probability of each pixel belonging to a specific class was estimated, and the pixels were assigned to their respective classes (Jensen 2015).

The samples were selected according to their location and respective classes. The samples for classification and validation were obtained from points collected in the field and supported by a QuickBird scene from 08/02/2008. Among the

five dates of TSX data, three were obtained during the fieldwork period (13/02/2016, 24/02/2016, and 06/03/2016), allowing the information contained in the images to be related to the field-collected data, thus enhancing the interpretation of the targets in the scenes (Figure 3).

Unlike the supervised method, in unsupervised classification, there is no prior determination of the classes to be classified. In this method, pixels are grouped according to the similarity in the backscattering patterns of surface targets, resulting in statistically grouped classes called clusters (Jensen 2015).

The unsupervised classification method used was ISODATA (Ball & Hall 1965). This method grouped the pixels into clusters according to the number of stipulated classes to determine which class the pixel would belong to and the number of times the algorithm should evaluate the pixel value in relation to existing class patterns on a given surface.

The surface zones extracted from SAR data were analyzed together with the DEM. This

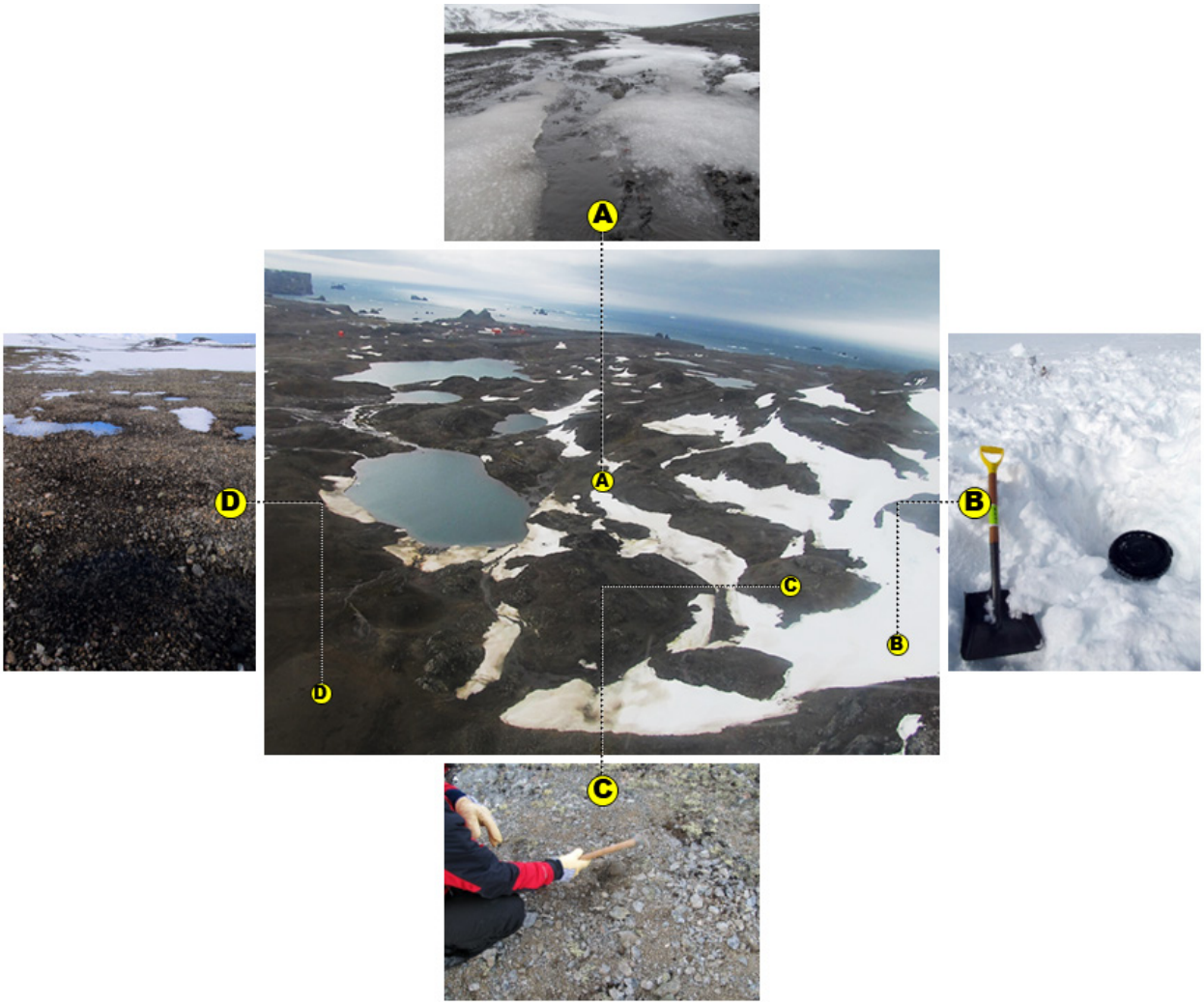

Figure 3. Example of samples used in the classification of targets in ice-free areas. a) Glaciofluvial channel on a surface with higher moisture content; b) Snow patch; c) Well-drained bare soil on a surface with lower moisture content; and d) Edge of soils with temporary hydromorphism on a surface transitioning in moisture content.

analysis made it possible to relate the SAR surface zones with the terrain shape and slope orientation.

To evaluate the accuracy of the classification, we used the indices of overall accuracy and kappa. The overall accuracy index was obtained by the ratio of the total number of correctly classified pixels to the total number of pixels that make up the confusion matrix of the classification. The kappa coefficient (Cohen 1960) was estimated by:

$$k = \frac{N\sum_{i=1}^{r} x_{ii} - \sum_{i=1}^{r} x_{i+} + x_{+i}}{N^2 - \sum_{i=1}^{r} x_{i+} + x_{+i}} \quad (1)$$

Where r is the number of rows or columns in the confusion matrix, x_{ii} is the number of observations on the diagonal of the matrix, x_{i+} is the sum of values in row i, x_{+i} is the sum of values in column i, and N is the total number of observations. According to Landis & Koch (1977), the kappa coefficient generates a value that, when compared to the kappa index, allows evaluating the quality of the classification. The index values were grouped as follows: <0.00 (Poor), 0.00 to 0.20 (Slight), 0.21 to 0.40 (Fair), 0.41 to 0.60 (Moderate), 0.61 to 0.80 (Substantial), and 0.81 to 1.00 (Almost Perfect) (Landis & Koch 1977).

For this, we used the data collected at the continuous monitoring site installed on Fildes Peninsula (Andrade et al. 2023), which collected data on air temperature, solar radiation, albedo, active layer moisture at 35 cm, and active layer temperature at 5 cm, 20 cm, and 35 cm depths. The average data for these variables were generated for the days when the TSX scenes were obtained, as well as for the 7 and 15 days preceding the acquisition of the TSX scenes (Table II). From this data, it was possible to assess the relationship between meteorological conditions and the backscattering patterns of surface targets in the TSX scenes.

The averages of the values of net radiation, albedo, active layer temperature, and active layer moisture in the months of February and March between 2014 and 2016 were quantified using the data collected by the continuous monitoring site (Andrade et al. 2023).

RESULTS AND DISCUSSION

The classification results varied according to the date and the method used (Table III). The overall accuracy index showed higher values than those acquired by the kappa index, a result similar to that obtained by Mora et al. (2017). However, the results of the kappa index are more consistent as they include all cells of the classification confusion matrix in the final result.

The kappa index in both classification methods indicates that the classifications were satisfactory, with a predominance of values in the strong and excellent classes, indicating consistency between what was classified and the field validation. Overall, the maximum likelihood method yielded better results, with four values rated as excellent and the remainder as strong. The ISODATA method also produced satisfactory results, with three values rated as excellent, six as strong, and only one as moderate.

The classification performance indices indicate higher accuracy in classifying targets on the glacier compared to targets in ice-free areas, a result similar to that obtained by Andrade et al. (2015). Due to the glacier surface being predominantly composed of snow and ice, the backscattering of these targets is more homogeneous, reducing the overlap of values in different targets. On the other hand, in the ice-free areas, where we observed greater heterogeneity of surface targets, there was greater overlap in backscattering values (Andrade et al. 2015). This overlap mainly occurred in targets with a high-water content in their compositions, such as bodies of water, melting snow, and bare soils in temporary hydromorphic conditions. The

Table II. Meteorological and thermal conditions of the active layer on the dates of obtaining the scenes and in the period of 7 and 15 days preceding the acquisition of the TerraSAR-X scenes.

	Dates	Air T.	Rn	Albedo	T 5 cm	M
		°C	Wm^{-2}		°C	%
Average for the day	10/3/14	0.47	78.58	0	1.58	13.18
	09/3/15	-0.47	66.90	0	1.21	18.94
	13/2/16	-0.21	75.22	0	0.83	13.10
	24/2/16	-0.58	81.85	0.19	N	14.45
	09/3/16	0.02	89.66	0	N	13.47
Average of the last 7 days	03/3 a 10/3/14	0.82	110.48	0.00	1.80	13.47
	02/3 a 09/3/15	0.25	68.18	0.03	1.19	18.92
	06/2 a 13/2/16	0.33	155.71	0.02	2.72	13.72
	17/2 a 24/2/16	0.24	97.05	0.09	N	14.20
	02/3 a 09/3/16	0.46	73.73	0.05	N	13.77
Average of the last 15 days	23/2 a 10/3/14	0.62	112.81	0.01	1.73	12.99
	22/2 a 09/3/15	-0.27	89.05	0.06	1.07	18.41
	29/1 a 13/2/16	0.61	156.68	0.04	2.92	13.78
	09/2 a 24/2/16	-0.18	126.13	0.03	1.64	13.82
	23/2 a 09/3/16	0.30	92.17	0.07	N	13.71

Air T: air temperature; Rn: net radiation; T 5 cm: active layer temperature at 5 cm depth; M: active layer moisture at 35 cm depth. N: no data.

electromagnetic radiation, when interacting with these targets that have liquid water, tended to scatter in a similar manner.

The land cover classes on the Fildes Peninsula exhibited high variability across the five dates, a condition supported by the coverage areas of each class (Table IV). During this period, there was greater variance in the glacier surface, with the highest variability in the wet snow class and the lowest variance in the bare ice class. The highest variance in the ice-free areas occurred in the moisture content transition class, while the lowest variance was in the surfaces with higher moisture content. This variability is influenced by the surface coverage of each class, considering that the largest variations occurred precisely in the classes with the largest coverage areas. In the ice-free areas, the transition class of moisture content stands out because meteorological variations significantly influenced the physical properties of seasonal snow, the thawing of the active layer, and the surface drainage flows resulting from the melting of snow and ice from different sources. Each factor mentioned contributed to the superiority of the transition class in moisture content in the ice-free areas.

In low-altitude glaciers influenced by maritime conditions, such as Collins Glacier, it is essential to monitor the variations that occur in their surface zones due to the proximity to the sea. The continuous increase in bare ice

Table III. Performance of Maximum Likelihood and ISODATA methods in classifying ice-free areas and glaciers in the five TerraSAR-X images.

		Maximum Likelihood		ISODATA	
		Overall accuracy (%)	Kappa	Overall accuracy (%)	kappa
Ice-free areas	10/03/2014	0.81	0.72	0.76	0.64
	09/03/2015	0.72	0.58	0.80	0.70
	13/02/2016	0.87	0.80	0.90	0.85
	24/02/2016	0.81	0.71	0.76	0.64
	06/03/2016	0.85	0.77	0.98	0.97
Glacier	10/03/2014	0.87	0.80	0.85	0.78
	09/03/2015	0.91	0.86	0.81	0.72
	13/02/2016	0.92	0.88	0.81	0.73
	24/02/2016	0.84	0.76	0.88	0.83
	06/03/2016	0.95	0.93	0.92	0.88

Table IV. Area of each land cover class in Fildes Peninsula on the five dates of TerraSAR-X data acquisition.

Class		Area (Km²)				
		10/03/2014	09/03/2015	13/02/2016	24/02/2016	06/03/2016
Glacier	Wet snow	13.3	19.9	14.1	17.7	19.5
	Transition: wet snow – bare ice	10.4	5.0	9.7	6.5	5.5
	Bare ice	2.0	0.7	1.9	0.5	0.8
Ice-free area	Higher moisture	2.1	2.7	3.5	5.9	4.8
	Transition in moisture	8.9	20.3	15.4	14.9	12.3
	Lower moisture	6.6	6.9	10.9	9.1	12.8

areas can be a negative indicator of glacier condition, considering that under unfavorable weather conditions, bare ice will tend to melt, leading to glacier retreat. On the other hand, the presence of wet snow can be a positive indicator because this class results from snowfall accumulated during autumn and winter (French 2007). Between March 2014 and March 2016, the Collins Glacier showed a trend of expansion in the wet snow surfaces and reduction in bare ice surfaces. The largest areas of bare ice surfaces occurred in March 2014, corresponding to 7.8% of the glacier area. In March 2015, there was an expansion of wet snow surfaces, covering 77.6% of the glacier surface, which contributed to overlapping the bare ice surfaces. The sequence of TSX data between 13/02/2016 and 06/03/2016 shows the high variability of surface zones, with the wet snow surface expanding in this short interval of 22 days, increasing from 54.7% to

75.6% of the total surface of the Collins Glacier. This expansion of the wet snow surface is influenced by the snowfall that occurred during this period. As March marks the end of summer, it consequently also ends the ablation period in this study area, it becomes crucial to map the surface dispersion of wet snow areas during this period, as there is a tendency for snowfall and accumulation to begin in the following months.

Due to the lower variance of targets in the ice-free areas, there was no class with a notable area variation during the study period. In the months of February and March, when intense ablation occurs, the predominant surface classes tend to be similar. Among the elements that compose the ice-free areas, snow is the most susceptible to meteorological variations, and after its melting, the surface becomes exposed. During these months, there is a high propensity for rock and bare soil to predominate, resulting in low variability of the classes. Due to this condition, the classification of surfaces emphasized the moisture content because of the low physical alternation of the constant targets, with moisture being the most differentiating factor in the physical condition of these targets.

The surface classes showed differences in their coverage areas on each of the classified dates, and to assess the predominant condition, we analyzed the intersection between the classified surfaces on each date, resulting in a surface containing the predominant condition over the period (Figure 4). The areas covered by the classes in the predominant condition follow the patterns already presented in the individual classifications. On the glacier, the class with the largest area was wet snow (85.5%), and the smallest area was bare ice (0.5%). In the ice-free areas, the predominant class was surfaces with lower moisture content (49.6%), while surfaces with higher moisture content were less represented (13%).

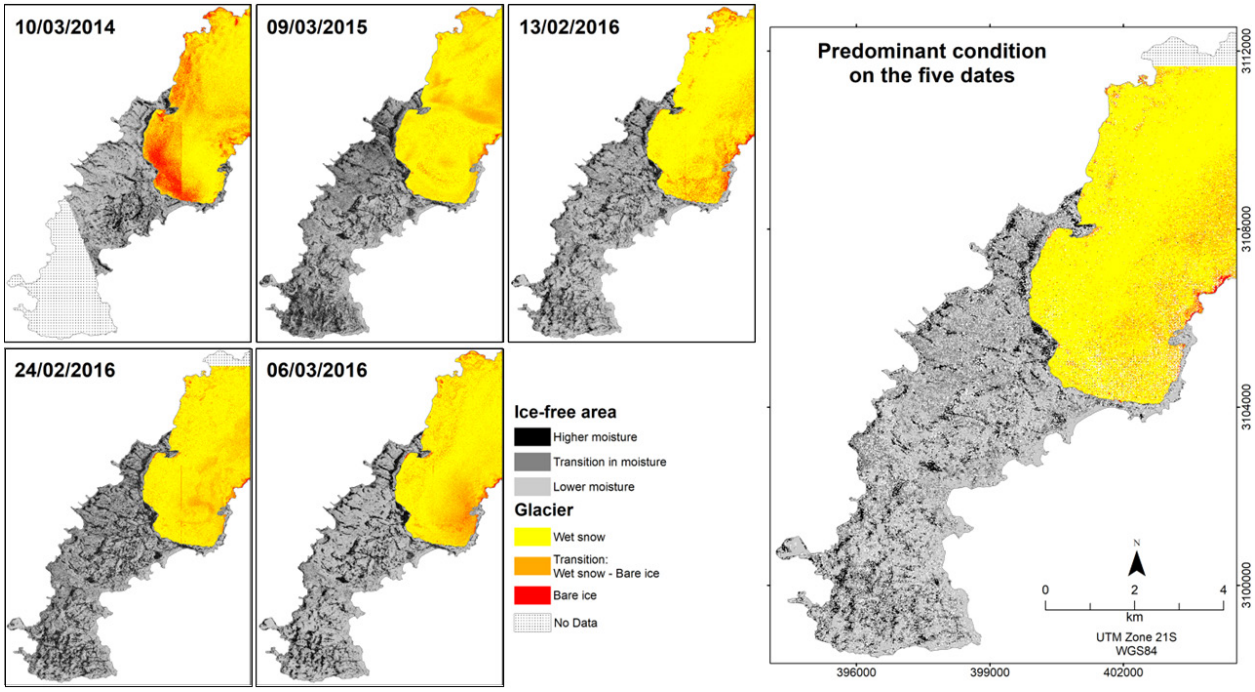

Figure 4. Surface coverage on the Fildes Peninsula generated from the classification of TerraSAR-X images and the predominant condition on the five dates.

The landforms, altitude, aspect, and slope influence surface targets (Rau et al. 2000, Andrade et al. 2015). The altitude of the part of the Collins Glacier covered in this study varies from 0 m at the parts of the glacier in contact with the sea to 250 m at the highest points. Through the intersection between the altitude data and the surface classified as predominant, we found that 75% of the bare ice surfaces are between 0 m and 50 m in altitude, while the classes of wet snow and the transition from wet snow to bare ice have about 45% of their areas between 100 m and 200 m in altitude. The predominance of the bare ice class near the sea is due to the influence of maritime conditions on the melting of snow and ice, while the predominance of wet snow at higher altitudes is due to favorable conditions for snow accumulation and less maritime influence. The slopes of the glacier also vary in their orientations, with 49.2% of the slopes of wet snow surfaces oriented to the northwest and 25.6% of the bare ice surfaces oriented to the southeast. In the Fildes Peninsula between 2012 and 2015, there was a predominance of northwest winds, and according to Turner & Pendlebury (2004), northwest winds generally transport warmer and moister air, whit the potential to accelerate the ablation process, while southeast and east winds transport colder and drier air.

The altitude in the ice-free areas varies from 0 m on the marine terraces to 180 m at the highest points on the plateaus. Based on the estimation of the predominant conditions of the classes in the ice-free areas, we observe that the three classes are more concentrated between 20 m and 60 m of altitude. The surfaces with lower moisture content, which are predominant, have a 58.8% occurrence in this altitude range. Regarding the orientation of the slopes, there was no prevailing direction in relation to the others; however, 50.8% of the surfaces with lower moisture content are located on slopes oriented to the northeast, south, and east, while the surfaces with higher moisture content are predominantly oriented to the west and southwest (44.8% of the total). The predominance of surfaces with lower moisture content is also influenced by winds that in these directions tend to be colder and drier. When we analyze the relationship between the predominant classes and the slope, we notice that in the ice-free areas, 55% of the area of each class is located on slopes between 3% and 20%, corresponding to the slightly undulated and undulated classes. However, there is no pattern in the slope indicating a significant contribution to the surface distribution of the predominant classes.

Backscattering of surface zones

From the classified areas, we obtained the characteristic backscattering values of each class. Surfaces with higher water content in liquid state exhibited lower backscattering due to electromagnetic radiation absorption. The lowest backscattering occurred on the wet snow surfaces of the glacier and on the surfaces with higher moisture content in the ice-free areas. A possible cause of the similarity was the presence of ice on the surface of the rocks, a condition observed during the fieldwork on 13/02/2016. After severe snowstorms, it is common to have ice cover on the surface, resulting in a scattering pattern on the rocks covered by ice that is similar to the pattern on the bare ice surfaces on the glacier. The scattering of snow varies according to its moisture content, composition, depth, surface roughness, and density (Albright et al. 1998).

Despite the bare ice surface and the surfaces with lower moisture content in the ice-free areas being very distinct, on 10/03/2014 and 13/02/2016 these classes had similar backscattering. It is

important to analyze the surface moisture content in ice-free areas, as this information allows us to infer the occurrence of permafrost, especially when the active layer is undergoing significant thawing. The Table V shows the mean values and standard deviation of backscattering extracted from the TSX scenes for each of the classes.

Other studies have used SAR data to assess the backscattering characteristics of cryosphere targets, with snow and ice being the most studied targets due to their wider coverage in this environment. Table VI provides a summary of backscattering values for the two classes, including the values obtained in this study and by other authors who used the C and X bands of SAR satellites.

The backscattering of surface targets varies according to the meteorological conditions preceding the image acquisition. Due to the high meteorological variability in the Maritime Antarctic region, it is important to evaluate the weather conditions preceding the acquisition of the scenes. So it is possible to relate the information from the image and assist in the correct interpretation of the targets classified in the images.

Air temperature strongly influences the melting of snow, ice, and consequently the active layer (Andrade et al. 2023). The average temperature for the months of February and March between 1968 and 2016 was 1.52°C and 0.39ºC, respectively. The air temperature in all TSX data obtained in February was below the historical average; however, the lowest air temperatures were recorded on the dates preceding the acquisition of the scene on 24/02/2016. The predominance of lower temperatures may be responsible for a larger area of wet snow on the glacier's surface and snow in ice-free areas. Among the scenes obtained in March, the one from 10/03/2014 was the only one with an average temperature higher than the historical temperature average on the date and in the period preceding the acquisition of the scene. The weather conditions

Table V. Backscattering from surface zones in the Fildes Peninsula generated from the TerraSAR-X temporal data series.

Surfaces zones		Backscattering (dB)									
		10/03/2014		09/03/2015		13/02/2016		24/02/2016		06/03/2016	
		SD	X	SD	X	SD	X	SD	X	SD	X
Glacier	Wet snow	-14.4	2.8	-19.1	5.1	-18.8	3.0	-19.6	3.8	-19.9	3.7
	Transition	-9.2	1.8	-13.6	3.3	-13.2	2.0	-14.1	3.6	-12.7	3.6
	Bare ice	-4.4	2.3	-2.4	6.3	-8.1	2.8	-7.3	8.1	-3.3	4.2
Ice-free area	Higher moisture	-14.8	3.2	-19.7	6.2	-19.7	3.7	-20.8	4.2	-20.1	4.4
	Transition in moisture	-10.0	2.6	-16.4	3.9	-15.2	2.7	-16.4	3.3	-14.9	3.0
	Lower moisture	-4.3	3.3	-10.7	4.3	-9.8	3.4	-10.6	3.8	-8.9	3.4

X: average; SD: standard deviation

on that date may have influenced the glacier's condition, with the largest areas of transition and bare ice. Due to the image obtained on that date not displaying the entire ice-free area, it is not possible to quantify the total influence of this condition on the classified targets. However, it is believed that on this date, there was a significant influence of weather conditions on the surface zones.

The average net radiation in the months of February and March was 128.5 Wm^{-2} e 68.85 Wm^{-2} respectively. On 03/10/2014, the net radiation was positive and higher than the average for the month of March during the study period. This indicates that there was a gain of energy and absorption of shortwave radiation incident on the targets, followed by the release of thermal energy. On 03/10/2014, an average albedo ranging from 0 to 0.01 was also recorded, indicating that the surface of the monitored area remained exposed and without the presence of targets with high reflection of radiation, causing a high absorption of incident radiation. The radiation balance above average on this date may have been influenced by the surface albedo. The average temperature in February and March between 2014 and 2016 was 1.90°C and 0.50°C respectively.

The active layer temperature at 5 cm depth on the dates of obtaining TSX data in March had values above the period's average, with the temperature on 03/10/2014 being 1.08°C higher than the March average. The active layer temperature at 5 cm depth on the dates of TSX data in March had values above the period's average, with 03/10/2014 standing out, where the temperature was 1.08°C higher than the March average. This set of variables indicates that among the five TSX scenes, the meteorological conditions most conducive to snow and ice melting occurred on 03/10/2014, while on the dates of 02/24/2016 and 03/06/2016, the

Table VI. Backscattering values obtained for the bare ice and wet snow surface zones in different studies.

Radar zones	[dB]	Band	Location	
Glacier: Bare ice	-15 a -10	C	Antarctic Peninsula	Rau et al. 2000
	-13 a -6	C	King George Island	M. Braun, unpublished data
	-13 a -6	C	Antarctic Peninsula	Arigony-Neto et al. 2009
	-19.2 a -10.1	X	Potter Peninsula	Andrade et al. 2015
	-19.9 a -14.6	X	Fildes Peninsula	This study
Glacier: Wet snow	~ -11	X	Everest Mountain	Albright et al. 1998
	-25 a -15	C	Antarctic Peninsula	Rau et al. 2000
	-22 a -15	C	King George Island	M. Braun, unpublished data
	-25 a -14	C	Antarctic Peninsula	Arigony-Neto et al. 2009
	-28.6 a -17.0	X	Potter Peninsula	Andrade et al. 2015
	-14.5 a -9.4	X	Fildes Peninsula	This study

meteorological conditions were conducive to less melting, causing a reduction in temperature and freezing of liquid water.

CONCLUSIONS

Using TerraSAR-X satellite images, we were able to extract backscattering signals and classify the different surface targets on the Fildes Peninsula. It was possible to classify the Fildes Peninsula into six classes of surface zones, three on the Collins Glacier and three in the ice-free areas. The high spatial resolution of TerraSAR-X was able to detect surface moisture and analyze the transition in moisture content, both on the glacier and in the ice-free areas. This was important for detecting surfaces in freezing or thawing conditions.

The results obtained in the classifications varied depending on the date, but all with the kappa index predominantly showing substantial and almost perfect values, highlighting the potential use of TerraSAR-X data for continuous monitoring of regions in the Maritime Antarctic. The glacier surface exhibited the greatest variability in surface targets, mainly in the wet snow surface class, which has the largest coverage area on the glacier, while in the ice-free areas, there was no class with prominent variability during the study period.

SAR radar satellites are important data sources for the continuous monitoring of surface zone variations in the Maritime Antarctic region. It's worth noting the possibility of obtaining data continuously regardless of weather conditions and solar illumination availability.

Acknowledgments

This study was supported by Coordenação de Aperfeiçoamento de Pessoal de Nível Superior (CAPES), CNPq/INCT 465680/2014-3, Instituto Nacional de Ciência e Tecnologia da Criosfera, PROANTAR, Marinha Brasileira, Universidade Federal do Rio Grande do Sul (UFRGS) and Universidade Federal de Viçosa (UFV).

REFERENCES

ALBRIGHT TP, PAINTER TH, ROBERTS DA & SHI J. 1998. Classification of surface types using SIR-C/X-SAR, Mount Everest Area, Tibet. J Geohys Res 103: 823-837.

ANDRADE AM, ARIGONY-NETO J, BREMER UF, MICHEL RFM, FASSONI-ANDRADE AC, SCHAEFER CEGR & SIMÕES JC. 2015. Cosmo-SkyMed X-band SAR data for classification of ice-free areas and glacier facies on Potter Peninsula, King George Island Antarctica. Geocarto Int 31: 803-812.

ANDRADE AM, MICHEL RFM, BREMER UF, LIMA NETO E, VIEIRA GBTG, SCHAEFER CEGR & SIMÕES JC. 2023. Thermal variations of the active layer in Fildes Peninsula, King George Island, Maritime Antarctica. An Acad Bras Cienc 95: e20230181.

ANDRADE AM, MICHEL RFM, BREMER UF, SCHAEFER CEGR & SIMÕES JC. 2018. Relationship between solar radiation and surface distribution of vegetation in Fildes Peninsula and Ardley Island, Maritime Antarctica. Int J Remote Sens 39: 2238-2254.

ARIGONY-NETO J, SAURER H, SIMÕES JC, RAU F, JAÑA R, VOGT S & GOßMANN H. 2009. Spatial and temporal changes in dry-snow line altitude on the Antarctic Peninsula. Clim Chang 94: 19-33.

BALL GH & HALL DJ. 1965. Isodata, a novel method of data analysis and pattern classification, California: Stanford Research Institute, 78 p.

BRAUN M, RAU F, SAURER H & GOßMANN H. 2000. Development of radar glacier zones on the King George Island ice cap, Antarctica, during austral summer 1996/97 as observed in ERS-2 SAR data. Ann Glaciol 31: 357-363.

COHEN JA. 1960. coefficient of agreement for nominal scales. Educ Psychol Meas 20: 37-46.

CURL JE. 1980. A Glacial History of the South Shetland Islands, Antarctica, Columbus: Ohio State University, 146 p.

DLR. 2010. TerraSAR-X Gound Segment: Basic Product Specification Document, 109 p.

FALK U, GIESEKE H, KOTZUR F & BRAUN M. 2016. Monitoring snow and ice surfaces on King George Island, Antarctic Peninsula, with high-resolution TerraSAR-X time series. Antartct Sci 28: 135-149.

FREEMAN A. 1992. Radiometric calibration of SAR image data. ISPRS, p. 212-222.

FRENCH HM. 2007. The Periglacial Environment, 480 p.

HUTCHINSON MF. 1989. A new procedure for gridding elevation and stream line data with automatic removal of spurious pits. J Hydrol (Amst) 106: 211-232.

IGM & INACH. 1996. Carta Topográfica, Instituto Geográfico Militar de Chile e Instituto Antártico Chileno.

JENSEN J. 2015. Introductory digital image processing: a remote sensing perspective. 658 p.

LANDIS J & KOCH G. 1977. The measurement of Oobserver Agreement for Categorical Data. Biometrics 33: 159-174.

MENDES JR CW, ARIGONY-NETO J, HILLEBRAND FL, FREITAS MWD, COSTI J & SIMÕES JC. 2022. Snowmelt retrieval algorithm for the Antarctic Peninsula using SAR imageries. An Acad Bras Cienc 94: e20210217.

MICHEL RFM, SCHAEFER CEGR, DIAS LE, SIMAS FNB, BENITES VM, MENDONÇA ES. 2006. Ornithogenic Gelisols (Cryosols) from Maritime Antarctica. Soil Sci Soc Am J 70: 1370-1376.

MICHEL RFM, SCHAEFER CEGR, MARTÍNEZ JL, SIMAS FNB, HAUS NW, SERRANO E & BOCKHEIM JG. 2014. Soils and landforms from Fildes Peninsula and Ardley Island, Maritime Antarctica. Geomorphology 225: 76-86.

MOORE ID, GRAYSON RB & LADSON AR. 1991. Digital Terrain Modelling: a review of hydrological, geomorphological, and biological applications. Hydrol Process 5: 3-30.

MORA C, JIMÉNEZ JJ, PINA P, CATALÃO J & VIEIRA G. 2017. Evaluation of single-band snow-patch mapping using high-resolution microwave remote sensing: an application in the maritime Antarctic. TC 11: 139-155.

ØVSTEDAL DO & SMITH RIL. 2001. Lichens of Antarctica and South Georgia: A guide to their Identification and Ecology, Cambridge: Cambridge University Press, 453 p.

PETER HU, BUESSER C, MUSTAFA O & PFEIFFER S. 2008. Risk assessment for the Fildes Peninsula and Ardley Island, and development of management plans for their designation as Specially Protected or Specially Managed Areas, Dessau-Roßlau: Umweltbundesamt Research Report, 508 p.

RAU F, BRAUN M, SAURER H, GOßMANN H, KOTHE G, WEBER F, EBEL M & BEPPLER D. 2000. Monitoring Multi-Year Snow Cover Dynamics on the Antarctic Peninsula Using SAR Imagery. Polarforschung 67: 27-40.

RICHARDS JA & JIA X. 2006. Remote Sensing Digital Image Analysis: An Introduction, Springer: Berlin, 454 p.

ROSA KK, PERONDI C, VEETTIL BK, AUGER JD & SIMÕES JC. 2020. Contrasting responses of land-terminating glaciers to recent climate variations in King George Island, Antarctica. Antartct Sci 32: 398-407.

SIEGERT M ETAL. 2019. The Antarctic Peninsula Under a 1.5°C Global Warming Scenario. Front Environ Sci 7: 1-7.

SIMÕES CL, ROSA KK, SIMÕES JC, VIEIRA R, COSTA RMC & SILVA AB. 2020. Recent changes in two outlet glaciers in the Antarctic Peninsula using multi-temporal Landsat and Sentinel-1 data. Geocarto Int 35: 1233-1244.

SKVARCA P & DE ANGELIS H. 2003. Impact assessment of regional climatic warming on glaciers and ice shelves of the northeastern Antarctic Peninsula. Antarct Penins Clim Variabil 79: 69-78.

TURNER J ET AL. 2013. Antarctic climate change and the environment: an update. Polar Rec 50: 1-23.

TURNER J & PENDLEBURY S. 2004. The International Antarctic Weather Forecasting Handbook, Cambridge: British Antarctic Survey, 685 p.

VIEIRA G, MORA C, PINA P & SCHAEFER CER. 2014. A proxy for snow cover and winter ground surface cooling: Mapping Usnea sp. communities using high resolution remote sensing imagery (Maritime Antarctica). Geomorphology 225: 69-75.

WEN J, KANG J, XIE Z, HAN J & ALBERT L. 1994. Climate, mass balance and glacial changes on small dome of Collins Ice Cap, King George Island, Antarctica. Antarct Res Book Ser 5: 52-61.

YUAN J, LV X & LI R. 2018. A Speckle Filtering Method Based on Hypothesis Testing for Time-Series SAR Images. Remote Sens 10: 1-21.

How to cite
DE ANDRADE AM, MICHEL RFM, DA ROSA KK, BREMER UF, SCHAEFER CEGR & SIMÕES JC. 2024. TerraSAR-X SAR data for classification of ice-free areas and glacier facies on Fildes Peninsula, King George Island, Antarctica. An Acad Bras Cienc 96: e20240362. DOI 10.1590/0001-3765202420240362.

Manuscript received on April 16, 2024;
accepted for publication on October 28, 2024

ANDRÉ M. DE ANDRADE[1]
https://orcid.org/0000-0003-3502-7847

ROBERTO F.M. MICHEL[2]
https://orcid.org/0000-0001-5951-4610

KÁTIA K. DA ROSA[3]
https://orcid.org/0000-0003-0977-9658

ULISSES F. BREMER[3]
https://orcid.org/0000-0003-0519-5807

CARLOS ERNESTO G.R. SCHAEFER[4]
https://orcid.org/0000-0001-7060-1598

JEFFERSON C. SIMÕES[3]
https://orcid.org/0000-0001-5555-3401

[1]Universidade Federal dos Vales do Jequitinhonha e Mucuri, Avenida Universitária, 1000, Bairro Universitário, 38620-870 Unaí, MG, Brazil

[2]Universidade Estadual de Santa Cruz, Rodovia Jorge Amado, Km 16, Salobrinho, 45662-900 Ilhéus, BA, Brazil

[3]Universidade Federal do Rio Grande do Sul, Avenida Bento Gonçalves, 9500, Agronomia, 91501-970 Porto Alegre, RS, Brazil

[4]Universidade Federal de Viçosa, Avenida Peter Henry Rolfs, s/n, Centro, 36570-900 Viçosa, MG, Brazil

Correspondence to: **André Medeiros de Andrade**
E-mail: andre.medeiros@ufvjm.edu.br

Author contributions

Performed field work and conceptualization: André Andrade, Roberto Michel, and Ulisses Bremer. Data analysis and wrote the paper: André Andrade, Roberto Michel, Kátia Rosa and Ulisses Bremer. Funding acquisition: Carlos Schaefer, Jefferson Simões and Ulisses Bremer.